
# LASER-INDUCED SPALL OF ALUMINUM AND ALUMINUM ALLOYS AT HIGH STRAIN RATES

D. A. Dalton, J. Brewer, A. C. Bernstein, W. Grigsby, D. Milathianaki, E. Jackson, R. Adams , P. Rambo, J. Schwarz, A. Edens, M. Geissel, I. Smith, E. Taleff, and T. Ditmire

Citation: AIP Conference Proceedings **955**, 501 (2007); doi: 10.1063/1.2833119

View online: http://dx.doi.org/10.1063/1.2833119

View Table of Contents:

http://scitation.aip.org/content/aip/proceeding/aipcp/955?ver=pdfcov

Published by the AIP Publishing

CP955, *Shock Compression of Condensed Matter - 2007,*
edited by M. Elert, M. D. Furnish, R. Chau, N. Holmes, and J. Nguyen


# LASER-INDUCED SPALL OF ALUMINUM AND ALUMINUM ALLOYS AT HIGH STRAIN RATES

**D.A. Dalton[1], J. Brewer[2,3], A.C. Bernstein[1], W. Grigsby[1], D. Milathianaki[1], E. Jackson[1], R. Adams[4], P. Rambo[4], J. Schwarz[4], A. Edens[4], M. Geissel[4], I. Smith[4], E. Taleff[2], and T. Ditmire[1]**

*[1]Dept. of Physics, University of Texas at Austin, 1 University Station C1600, Austin, TX 78712*
*[2]Dept. of Mechanical Engineering, University of Texas at Austin, 1 University Station C2200, Austin, TX 78712*
*[3]Present Address: Stress Engineering Services, Inc., 13800 Westfair East Drive, Houston, TX 77041*
*[4]Sandia National Laboratories, Z-Backlighter Facility, Albuquerque, NM 87185*

**Abstract.** We conducted laser-induced spall experiments aimed at studying how a material's microstructure affects the tensile fracture characteristics at high strain rates (>$10^6$ $s^{-1}$). We used the Z-Beamlet Laser at Sandia National Laboratory to drive shocks and to measure the spall strength of aluminum targets with various microstructures. The targets were recrystallized, high-purity aluminum (Al-HP RX), recrystallized aluminum + 3 wt.% magnesium (Al-3Mg RX), and cold-worked aluminum + 3 wt.% magnesium (Al-3Mg CW). The Al-3Mg RX and Al-3Mg CW are used to explore the roles that solid-solution alloying and cold-work strengthening play in the spall process. Using a line-VISAR (Velocity Interferometer System for Any Reflector) and analysis of recovered samples, we were able to measure spall strength and determine failure morphology in these targets. We find that the spall strength is highest for Al-HP RX. Analysis reveals that material grain size plays a vital role in the fracture morphology and spall strength results.

**Keywords:** Aluminum, VISAR, spall, fracture.
**PACS:** 42.79.Qx, 62.20.-x.

## INTRODUCTION

Spall is the planar fracture of material at fast strain rates due to a tensile stress, such as that initiated by explosives, plate impacts, or pulsed laser irradiation. When an intense laser irradiates a solid target, an ablation-driven shock-wave propagates through the material, reflects off the rear (free) surface and produces a rarefaction wave back into the target. The material is put into tension as this rarefaction wave encounters the rarefaction from the decay of the still forward-going shock. When the resulting tensile stress surpasses the maximum tensile strength for the material under the given loading conditions, the material will spall.

A great deal of experimental work has been performed, measuring spall strength of materials with different microstructures over the strain rates accessible with gas guns and flyer plates, specifically strain rates of $10^4$-$10^6$ $s^{-1}$. Various studies have investigated microstructural influences on spall strength including grain size [1, 2], second-phase particles [3], alloying [4], and grain orientation [1, 4]. Laser driven shock experiments have the interesting feature that they

can access strain rates much faster than is possible with flyer-plate-driven experiments. More recently, using a line-VISAR probe coupled with drive lasers of various pulse durations, Moshe, *et al.* were able to study spall strength over a range of very high strain rates. They showed that laser-driven foils of aluminum and copper exhibited spall strength that dramatically increases with strain-rate above $10^7$ $s^{-1}$ [5, 6]. This result implied a change in spall failure mechanism at strain rates around $10^7$ $s^{-1}$.

Furthermore, the effect of grain size on spall strength has not been well established in the literature. Some groups have found that spall strength increases as grain size decreases [2], while others have found that spall strength increases with increasing grain size [1]. Using a laser-driven mini-flyer system, Robbins, *et al.* showed that cold-rolled copper targets had lower spall strength than annealed copper; however, in that study specimen purity may have been a contributing factor [7].

To investigate these physical attributes at very high strain rate in a systematic way, we report on the spall strength and fracture morphology of aluminum slabs subject to strain rates of 2 – 8 x $10^6$ $s^{-1}$. Slabs of pure Al-HP RX, Al-3Mg RX, and Al-3Mg CW were shock-driven using the Z-Beamlet Laser at Sandia National Laboratory. A line-VISAR diagnostic was used to infer the spall strength of the materials and post-shot target analysis explored the microscopic fracture morphology.

## EXPERIMENTAL PROCEDURE

The Z-Beamlet Laser is a 1.2 kJ laser of frequency-doubled light at 527 nm and pulse length of 1.8 ns. The pulse shape was square and had a top-hat intensity profile. The laser was focused with an f/8 optic and the target was placed ~50 mm from focus to give a spot size of 4-10 mm wide.

The target thicknesses used in our experiments were 200 μm and 500 μm. The 200 μm targets were impacted at (3.4-5.7)x$10^{11}$ W/$cm^2$ and produced a strain rate of ~6x$10^6$$s^{-1}$. The 500 μm targets were impacted at (1.0-1.5)x$10^{12}$ W/$cm^2$ and produced a strain rate of ~2x$10^6$ $s^{-1}$. We ran HYADES simulations to determine the pressure range of our experiments. For the 200 μm (500 μm) targets, the pressure near the rear surface was 65-100 kbar (65-80 kbar) [8].

The long pulse probe is a line-VISAR diagnostic which is used to measure the free surface velocity of our target. Light reflecting from a moving surface produces Doppler shifted light which is interfered with itself at a later time to produce temporal interference where the fringe shifts are proportional to the free surface velocity. The VISAR diagnostic closely follows the design features of Celliers, *et al.* [9]. The line-VISAR probe beam is produced by a single-longitudinal mode laser (Spectra-Physics Lab-130 Laser, 532 nm, ~80 mJ, 8 ns FWHM) and a pulse stacker is used to elongate the pulse to 30 ns [10]. Further experimental details can be found elsewhere [11].

## RESULTS AND DISCUSSION

### Spall Strength Results

The free-surface velocity is determined by analyzing the relative phase of the line-VISAR interferogram. The velocity-per-fringe constant is defined as:

$$VPF_0 = \frac{\lambda}{2\tau(1+\delta)} = \frac{\lambda c}{4h\left(n-\frac{1}{n}\right)(1+\delta)} \quad (1)$$

where $\lambda$, $\tau$, $h$, $n$, and $(1+\delta)$ are laser wavelength, temporal delay of etalon, etalon thickness, index of refraction of etalon, and etalon dispersion.

An example interferogram is shown in Fig. 1 along with a velocity vs. time lineout. The interferograms were analyzed using a Fourier transform method to extract the phase [9]. A range of interest from a relatively flat area of breakout was selected from the interferogram. The phase map is multiplied by the velocity-per-fringe constant to extract a velocity map. Because of the uneven spatial breakout, we took four velocity lineouts over our region of interest.

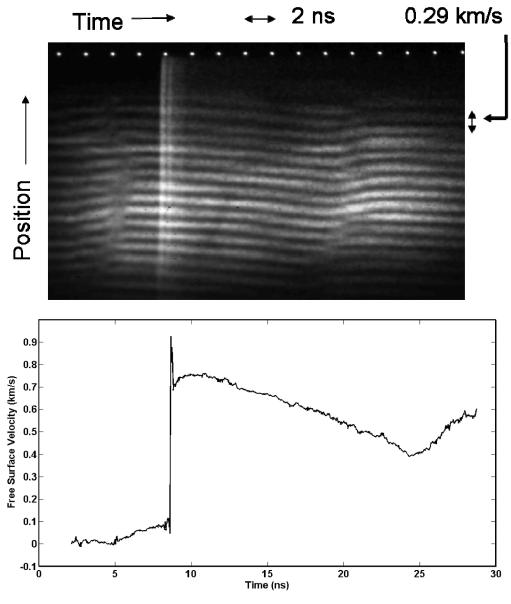


**Figure 1.** A line-VISAR interferogram and a resulting velocity versus time lineout extracted using Fourier Transform analysis. The velocity per fringe constant is 0.29 km/s/fringe.

A polynomial fit is applied after shock breakout for each lineout to get a smooth velocity profile. Extracting the maximum and minimum velocities, we determine the spall strength and strain rate for each lineout using:

$$P_{spall} = \tfrac{1}{2}\rho_0 \cdot c \cdot \Delta u \qquad (2)$$

$$\dot{\varepsilon} = \frac{\Delta u}{\Delta t} \cdot \frac{1}{2c} \qquad (3)$$

where $\rho_0$, $c$, $\Delta u$, and $\Delta t$ are density, bulk sound speed, pullback velocity, and the difference in time related to the pullback velocity.

We then averaged the spall strength and strain rate values for the lineouts. Fig. 2 shows the data for spall strength versus strain rate against data from Moshe, *et al.* [5, 6]. The error bars are derived from the standard deviation in spall strength and strain rate over multiple equally spaced lineouts.

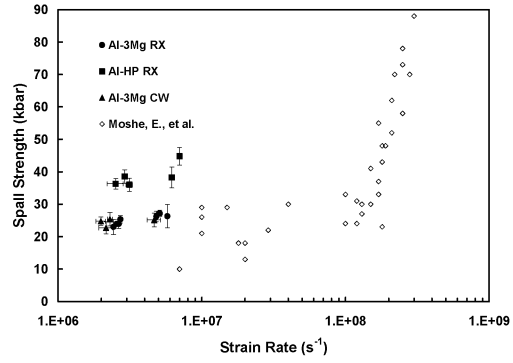


**Figure 2.** Spall strength versus strain rate data for Al-HP RX, Al-3Mg RX, and Al-3Mg CW shown together with data from Moshe, *et al.* [5, 6].

## Post-Shot Spall Samples

Fig. 3 shows SEM images of the failure surface of (a) Al-HP RX and (b) Al-3Mg CW. The prominent feature in the Al-HP RX is transgranular, ductile dimpling. For Al-3Mg CW the dominant failure mode is brittle, intergranular fracture. Further details regarding the post-shot analysis of the targets can be found elsewhere [12].

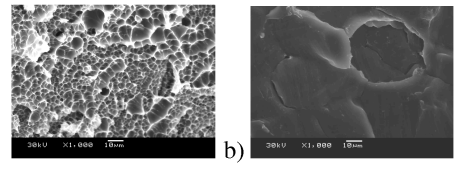


**Figure 3**. The SEM images show the exposed spall plane for (a) Al-HP RX and (b) Al-3Mg CW.

## Discussion

The Al-HP RX spall strength values are high for this strain rate as compared to Moshe [5, 6] and Robinson [13]. We do not know all the details regarding sample preparation in these previous publications. Al-3Mg RX and CW showed slight differences in spall strength, which contradicts results for copper in Robbins, *et al.* that shows a significant difference in spall strength between the annealed and cold-rolled copper [7].

Upon analysis, the recrystallized aluminum showed large average grain size, probably explaining our measured large spall strength relative to the aluminum alloy that had smaller grains. The grain size was smaller and similar in size for both the recrystallized and cold-worked Al-3 Mg. The spall strength of the alloys was likely lowered by the fact that there was more surface area at grain boundaries at which voids could form, as suggested by Minich [1].

## CONCLUSIONS

At engineering strain rates stronger materials can be engineered in various ways, i.e. grain size reduction, solid-solution alloying, and cold-working. We wanted to determine how material microstructure would affect spall strength at the high strain rates reached with the Z-Beamlet Laser, and we saw that grain size plays a vital role in the failure mechanism. Furthermore, material characterization and analysis at these higher strain rates is crucial to explaining our dynamic strength measurements.

## ACKNOWLEDGEMENTS

The authors would like to thank Jeff Colvin, Ray Smith, and many other people at Lawrence Livermore National Laboratory. This work was supported by the Army Research Office and the National Nuclear Security Administration under cooperative agreement DE-FC52-03NA00156. Sandia is a multiprogram laboratory operated by Sandia Corporation, a Lockheed Martin Company, for the United States Department of Energy's National Nuclear Security Administration under contract DE-AC04-94AL85000.

## REFERENCES

1. Minich, R.W., et al.. "Effect of Microstructural Length Scales on Spall Behavior of Copper", Metall. Mater. Trans. A **35**, 2663 (2004).
2. Buchar, J., Elices, M., and Cortez, R., "The Influence of Grain Size on the Spall Fracture of Copper", J. Phys. IV, **1**, C3-623 (1991).
3. Jacobi, S., Zaretsky, E., and Shvarts, D., "Experimental study and modeling of dynamic fracture of copper", in *Fundamental Issues and Applications of Shock-Wave and High-Strain-Rate Phenomena*, edited by Staudhammer, K. P., Murr, L. E., and Meyers, M. A., (Elsevier, New York, NY, 2001), p. 525.
4. Chen, X., et al., "Spall behavior of aluminum with varying microstructures", J. Appl. Phys. **99**, 023528 (2006).
5. Moshe, E., et al., "An increase of the spall strength in aluminum, copper, and Metglas at strain rates larger than $10^7$ $s^{-1}$", J. Appl. Phys. **83**, 4004 (1998).
6. Moshe, E., et al., "Experimental measurement of the strength of metals approaching the theoretical limit predicted by the equation of state", Appl. Phys. Lett. **76**, 1555 (2000).
7. Robbins, D. L., et al., Los Alamos Technical Report No. LA-14150, 2004.
8. Larsen, J. T., and Lane, S. M., "Hyades- a Plasma Hydrodynamics Code for Dense-Plasma Studies", J. Quant. Spect. & Rad. Transfer, **51**, 179 (1994).
9. Celliers, P. M., et al., "Line-imaging velocimeter for shock diagnostics at the OMEGA laser facility", Rev. Sci. Instrum. **75**, 4916 (2004).
10. Bernstein, A. C., et al., (to be submitted)
11. Dalton, D. A., et al., (to be submitted)
12. Brewer, J. L., et al., "Influence of Microstructure on the Spall Failure of Aluminum Materials", Metall. Mater. Trans. A (accepted).
13. Robinson, C. M., "Modeling of Laser Spall Experiments on Aluminum," in Shock Compression of Condensed Matter-2001, edited by Furnish, M. D., Thadhani, N. N., and Horie, Y., (American Institute of Physics, Melville, N.Y., 2002), pp. 1359-1362.